Analysis of Second-Order Intermodulation in Miller Bandpass Filters

Joung Won Park, *Member, IEEE*, and Behzad Razavi, *Fellow, IEEE*

***Abstract*—Miller bandpass filters combine the properties of N-path circuits with the Miller effect to achieve a narrow bandwidth and high out-of-channel rejection. This brief investigates the second-order intermodulation behavior of such filters in the context of direct-conversion receivers. It is shown that the second intercept point rises by an amount equal to the circuit's out-of-channel rejection.**

***Index Terms*—intermodulation, Miller bandpass filter (MBPF), N-path filter, second-order intermodulation ($\mathbf{IM_2}$) mitigation.**

I. Introduction

THE Miller bandpass filter (MBPF) [1] is an N-path topology that can achieve a much narrower bandwidth and operate with smaller switches than conventional designs. Providing bandwidths as narrow as a few hundred kilohertzs at a center frequency of 1 or 2 GHz [1], this topology can attenuate both close-in and far-out blockers. One may then surmise that Miller filtering can improve the second intercept point (IP_2).

This brief analyzes the behavior of MBPFs with respect to second-order intermodulation (IM_2) effects. It is proved that the IP_2 indeed increases according to the out-of-channel attenuation provided by the MBPF.

II. Background

Fig. 1(a) shows a simple "commutated network," which is also known as an N-path filter. As shown by Smith in 1953 [2], the periodic nonoverlapping switching of the capacitors translates the transfer function of the original continuous-time circuit to a center frequency equal to the switching rate, i.e., f_{LO}. Smith also pointed out that the bandwidth of the resulting bandpass response is approximately equal to $(NR_SC_u)^{-1}$, where N denotes the number of unit capacitors [and the local oscillator (LO) phases]. From another perspective, the bandwidth is inversely proportional to the total capacitance and independent of the number of phases.

Manuscript received January 15, 2016; revised March 15, 2016; accepted April 3, 2016. Date of publication April 21, 2016; date of current version February 24, 2017. This brief was recommended by Associate Editor Z. Galias.

J. W. Park is with the Research and Development, Qualcomm Technologies, Inc., San Diego, CA 92121 USA (e-mail: joungwon@ucla.edu).

B. Razavi is with the Electrical Engineering Department, University of California at Los Angeles, Los Angeles, CA 90095 USA (e-mail: razavi@ee.ucla.edu).

Color versions of one or more of the figures in this brief are available online at http://ieeexplore.ieee.org.

Digital Object Identifier 10.1109/TCSII.2016.2555930

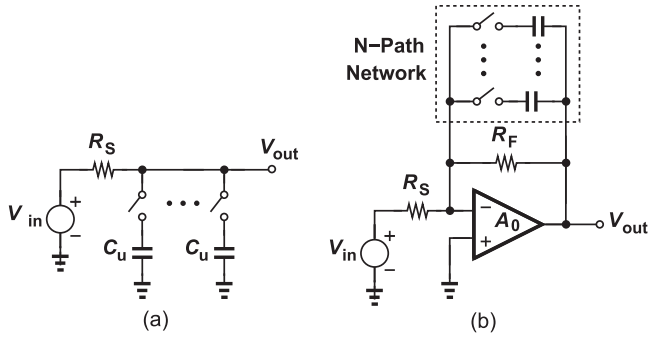

Fig. 1. (a) N-path filter. (b) MBPF.

The MBPF exploits the Miller effect to increase the apparent value of the capacitors in an N-path circuit, thus providing a narrower bandwidth for a given amount of capacitance. As shown in Fig. 1(b), the MBPF consists of an N-path network placed around an amplifier, presenting a bandwidth of approximately $[2\pi R_S N(1+A_0)C_u]^{-1}$. It is also shown that the on-resistance of the switches in the feedback path is divided by $1+A_0$, improving the out-of-channel rejection [1]. The resistor R_F establishes input matching within the desired channel. In this brief, we assume ideal switches and $N=4$. The analysis is carried out for a single-ended amplifier, but the results also apply to a differential front end (with random asymmetries).

III. Analysis Procedure

Let us model the amplifier in Fig. 1(b) by a second-order nonlinearity of the form $y=\alpha_1 x+\alpha_2 x^2$, where $\alpha_1=A_0>0$. Here, we assume that the amplifier is weakly nonlinear so that the x^4 and higher-order terms are negligible [3]. The overall front end is therefore a dynamic nonlinear system that can be analyzed by harmonic balance methods. For IM_2 analysis, we apply to the input two equal tones at ω_1 and ω_2 outside the passband and assume an output IM_2 of the form $V_{\mathrm{IM2}}\cos[(\omega_1-\omega_2)t+\theta]$, where V_{IM2} and θ are unknown. Our harmonic balance analysis exploits the method of "nonlinear currents" [4] and proceeds in five steps: 1) assume that the amplifier is negligibly compressed and compute the magnitude of the main tones at the output; 2) return these tones and $V_{\mathrm{IM2}}\cos[(\omega_1-\omega_2)t+\theta]$ to the virtual ground by proper transfer functions; 3) allow the main tones at the virtual ground to travel through the amplifier and generate an IM_2 product; 4) allow the IM_2 component at the virtual ground to be amplified by the small-signal gain;

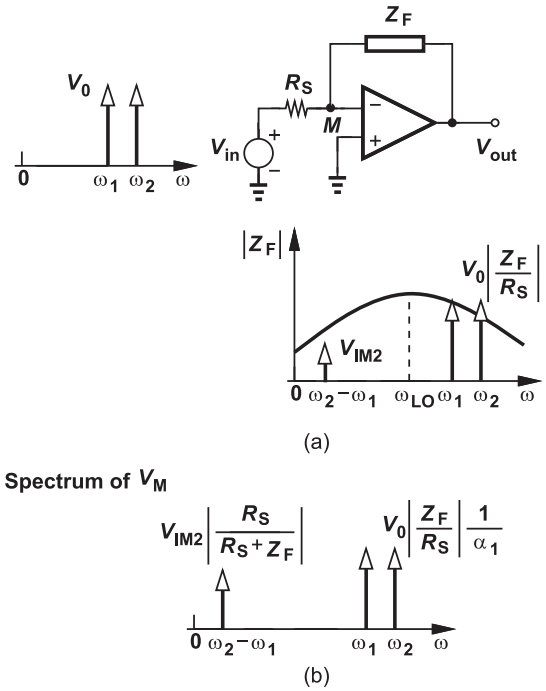

Fig. 2. (a) Frequency response of a nonlinear amplifier with frequency-dependent feedback impedance. (b) Frequency spectrum at node M.

and 5) equate the sum of the IM_2 components computed in the last two steps to the original output IM_2, i.e., $V_{IM2}\cos[(\omega_1 - \omega_2)t + \theta]$, obtaining V_{IM2} in terms of known quantities.

IV. Continuous-Time Approximation

Since the N-path network in Fig. 1(b) acts as a bandpass impedance, we intuitively expect that we can approximate it by a continuous-time equivalent. Here, we model the entire feedback network by a continuous-time impedance Z_F and, as shown in Fig. 2(a), apply two closely spaced tones at the input. The output thus contains the main tones and an IM_2 component at $\omega_2 - \omega_1$.

For our harmonic balance analysis, we make the following simplifying assumptions: the amplifier has a high gain and a low output impedance and Z_F has approximately the same magnitude and phase at ω_1 and ω_2 because $\omega_2 - \omega_1$ is small. If $V_{in} = V_0\cos\omega_1 t + V_0\cos\omega_2 t$ and the amplifier gain is high, the main tones experience a transfer function given by $-Z_F/R_S$ and emerge at the output as

$$V_{out,\omega 1,\omega 2}(t) = -V_0\left|\frac{Z_F(\omega_1)}{R_S}\right|[\cos(\omega_1 t+\phi)+\cos(\omega_2 t+\phi)] \quad (1)$$

where we have assumed $|Z_F(\omega_1)| \approx |Z_F(\omega_2)|$ and $\angle Z_F(\omega_1) \approx \angle Z_F(\omega_2) = \phi$.

In order to compute V_{IM2}, we allow the output components to circulate around the loop, i.e., we refer them to node M and subject the results to the amplifier characteristic, i.e., $\alpha_1 x + \alpha_2 x^2$. An interesting and critical point here is that the output IM_2 product and the main tones are referred to M by *different* transfer functions. This is because V_{in} itself contains no signal at $\omega_2 - \omega_1$. Consequently, the IM_2 component is simply divided by R_S and Z_F as it returns to M, i.e.,

$$V_{M,IM2}(t) = \frac{R_S}{|R_S + Z_F(\omega_2-\omega_1)|} \times V_{IM2}\cos[(\omega_1-\omega_2)t+\theta+\beta] \quad (2)$$

where β is the phase contributed by the voltage divider $R_S/|R_S + Z_F(\omega_2 - \omega_1)|$. Note that Z_F in (2) is calculated at $\omega_1 - \omega_2$ and, owing to its bandpass nature, is very small. On the other hand, to refer the main tones to M, we divide their magnitude by the amplifier gain α_1 [see Fig. 2(b)], i.e.,

$$V_{M,\omega 1,\omega 2}(t) = \frac{V_0}{\alpha_1}\frac{|Z_F(\omega_1)|}{R_S}[\cos(\omega_1 t+\phi)+\cos(\omega_2 t+\phi)]. \quad (3)$$

In the next step of the harmonic balance analysis, we allow $V_{M,IM2}(t)$ to be amplified by a factor of α_1 and $V_{M,\omega_1,\omega_2}(t)$ to experience the amplifier nonlinearity and hence generate IM_2. The sum of these output IM_2 components is then equated to our original expression $V_{IM2}\cos[(\omega_1 - \omega_2)t + \theta]$, i.e.,

$$\begin{aligned}&\frac{\alpha_2 V_0^2}{\alpha_1^2}\frac{|Z_F(\omega_1)|^2}{R_S^2}\cos(\omega_1-\omega_2)t \\ &\quad - \alpha_1\frac{R_S}{|R_S+Z_F(\omega_2-\omega_1)|}V_{IM2}\cos[(\omega_1-\omega_2)t+\theta+\beta] \\ &\quad = V_{IM2}\cos[(\omega_1-\omega_2)t+\theta]. \end{aligned} \quad (4)$$

Recognizing that $R_S/|R_S + Z_F(\omega_2 - \omega_1)| \approx 1$ and $\alpha_1 \gg 1$, we obtain

$$\alpha_1 V_{IM2}\cos[(\omega_1-\omega_2)t+\theta+\beta] = \frac{\alpha_2 V_0^2}{\alpha_1^2}\frac{|Z_F(\omega_1)|^2}{R_S^2}\cos(\omega_1-\omega_2)t. \quad (5)$$

For this relationship to hold at all t, the amplitudes must be equal, and hence

$$|V_{IM2}| = \frac{\alpha_2}{\alpha_1^3}\frac{|Z_F(\omega_1)|^2}{R_S^2}V_0^2. \quad (6)$$

This result suggests that if Z_F in Fig. 2(a) attenuates the two tones by a factor of $k = |Z_F(\omega_1)/R_S|$ with respect to the peak at ω_{LO}, then V_{IM2} falls by a factor of k^2 and the IP_2 rises by a factor of k. The key point offered by our analysis is that a bandpass network placed around an amplifier can raise the IP_2. On the other hand, if Z_F is a simple resistor and much greater than R_S, then we can rewrite $|V_{IM2}|$ as

$$|V_{IM2}| = \frac{\alpha_2}{\alpha_1^2}\frac{|Z_F(\omega_1)|^2}{R_S^2}\frac{1}{\frac{\alpha_1 R_S}{|Z_F(\omega_2-\omega_1)|}+1}V_0^2. \quad (7)$$

Equation (7) indicates that $|V_{IM2}|$ is suppressed by only a factor of $\alpha_1^3(R_S/|Z_F(\omega_2 - \omega_1)| + 1/\alpha_1)$, which can be much smaller than α_1^3 in (6).

In our study, we examine the spectrum at the output of the amplifier in Fig. 1(b) to measure the (low-frequency) IM_2

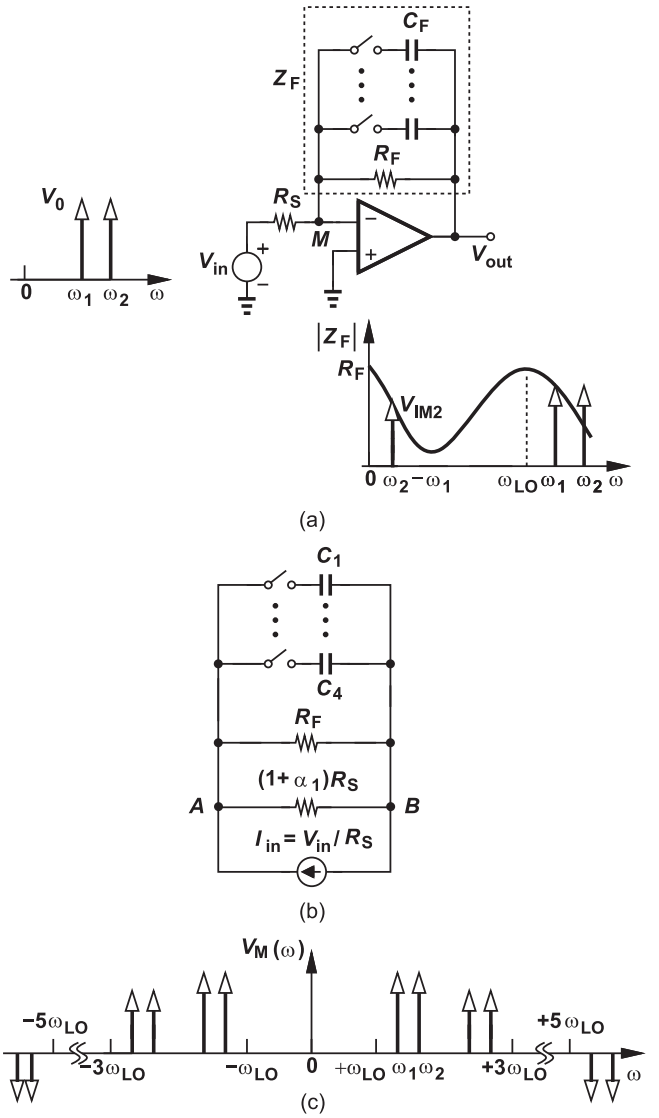

Fig. 3. (a) Frequency response of a nonlinear amplifier with an N-path filter in feedback. (b) Frequency spectrum at node M.

component. The receiver IP_2, however, also depends on the mismatches within the downconversion circuit, which can be either an explicit stage following this front end or simply embedded within the N-path filter [1]. In other words, the results of our study must be scaled according to the downconversion circuit mismatches to yield the overall IP_2.

V. Discrete-Time Feedback

While intuitive and mathematically efficient, the continuous-time approximation disregards various mixing products that are generated within the feedback N-path network, casting doubt on the validity of (6). We must compute both the main tones and the IM_2 product for the discrete-time system.

A. Main Tones at Output

To determine the amplitude of the main tones, we first replace $V_{\rm in}$, R_S, and the amplifier in Fig. 3(a) with their Norton equivalent [see Fig. 3(b)]. We also recognize that $|Z_F|$ in Fig. 3(a) rises as ω approaches zero. Note that $C_1 = \cdots = C_4 = C_F$, and $R_F = (1+\alpha_1)R_S$ is necessary for input matching [see Fig. 3(a)]. The impedance presented to $I_{\rm in}$ has been calculated in [5] and, in the vicinity of $\omega_{\rm LO}$, can be simplified to

$$\begin{aligned} Z_{AB} &\cong \left[\frac{8}{\pi^2}\frac{(1+\alpha_1)R_S}{2}\right] \| \left[Z_4(\omega-\omega_{\rm LO})\right] \\ &= \left[\frac{8}{\pi^2}\frac{(1+\alpha_1)R_S}{2}\right] \| \left[\frac{2}{\pi^2}\frac{1}{jC_F(\omega-\omega_{\rm LO})}\right] \end{aligned} \tag{8}$$

where $(1+\alpha_1)R_S$ is divided by 2 to account for R_F, and Z_4 denotes the impedance of the four commutated capacitors. Writing $V_{AB} = I_{\rm in}Z_{AB}$ and noting that $V_{\rm out}$ in Fig. 3(a) is simplified to $[\alpha_1/(\alpha_1+1)]V_{AB}$, we obtain the transfer function as

$$\frac{V_{\rm out}}{V_{\rm in}} = \frac{4}{\pi^2}\frac{1+\alpha_1}{1+2j(1+\alpha_1)R_SC_F(\omega-\omega_{\rm LO})}. \tag{9}$$

If the tones lie outside the passband, then $|\omega-\omega_{\rm LO}|^2 \gg 1/[2(1+\alpha_1)R_SC_F]^2$ and

$$\left|\frac{V_{\rm out}}{V_{\rm in}}\right| \approx \frac{2}{\pi^2}\frac{1}{R_SC_F(\omega-\omega_{\rm LO})} \approx \frac{|Z_4(\omega-\omega_{\rm LO})|}{R_S}. \tag{10}$$

For a two-tone input, we thus have

$$V_{\rm out}(t) = -V_0\frac{|Z_4|}{R_S}\left[\cos(\omega_1 t+\theta)+\cos(\omega_2 t+\theta)\right] \tag{11}$$

where $|Z_4(\omega_1)| \approx |Z_4(\omega_2)|$, and $\angle Z_4(\omega_1) \approx \angle Z_4(\omega_2) = \theta$.

B. Feedback Components

We now return the output tones and the IM_2 components to node M in Fig. 3(a). The former are divided by the amplifier gain in a manner similar to (3), i.e.,

$$V_{M,\omega_1,\omega_2}(t) = \frac{V_0}{\alpha_1}\frac{|Z_4|}{R_S}\left[\cos(\omega_1 t+\theta)+\cos(\omega_2 t+\theta)\right] \tag{12}$$

where Z_4 is evaluated at $\omega_1 \approx \omega_2$.

We must add the mixing products as well to the preceding value. Specifically, the main output tones mix with $4\omega_{\rm LO}$, $8\omega_{\rm LO}$, etc., as they return to M. As depicted in Fig. 3(c), the resulting spectrum contains these components with declining amplitudes, for example, $V_M(4\omega_{\rm LO}-\omega_1) = (1/3)V_M(\omega_1)$ and $V_M(4\omega_{\rm LO}+\omega_1) = (1/5)V_M(\omega_1)$ [6]. This is the first difference between the continuous- and discrete-time models.

The output IM_2 component propagates through the N-path impedance, with this impedance evaluated at $\omega_1-\omega_2$; as depicted in Fig. 3(a), this impedance has a *high* value if $\omega_1-\omega_2$ is small. We expect that the four capacitors present an overall impedance of $[4C_F(\omega_1-\omega_2)]^{-1}$ at low frequencies, attenuating the IM_2 component by a factor of $R_S/\{R_S+R_F\|[4C_F(\omega_1-\omega_2)]^{-1}\}$. This is the second difference between the continuous- and discrete-time models. It follows that the IM_2 returned to the virtual ground is given by:

$$\begin{aligned} V_{M,\rm IM2}(t) = &\frac{R_S}{\left|R_S+\frac{R_F}{1+4jR_FC_F(\omega_1-\omega_2)}\right|} \\ &\times V_{\rm IM2}\cos\left[(\omega_1-\omega_2)t+\theta+\beta\right]. \end{aligned} \tag{13}$$

Since $R_F = (1+\alpha_1)R_S \gg R_S$, this result can be simplified if $\omega_1 - \omega_2$ is small, i.e.,

$$V_{M,\mathrm{IM2}}(t) = \frac{1}{1+\alpha_1} V_{\mathrm{IM2}} \cos\left[(\omega_1-\omega_2)t + \theta + \beta\right]. \quad (14)$$

One may wonder whether the output IM_2 component in Fig. 3(a) is mixed with the LO phases as it returns through the N-path network, i.e., whether it manifests itself at $\omega_{\mathrm{LO}} \pm (\omega_2 - \omega_1)$ at node M. Indeed, the mixing occurs, but with perfectly matched paths, the upconverted phases of V_{IM2} exactly cancel as they reach this node.

C. IM_2 Product at Output

In a manner similar to the continuous-time approximation, we allow the components at node M in Fig. 3(a) to propagate through the amplifier: the main tones around ω_{LO}, $3\omega_{\mathrm{LO}}$, etc., experience the second-order nonlinearity, generating IM_2, whereas the IM_2 component at M is simply amplified by a factor of α_1. In order to compute the IM_2 product resulting from the main tones, we calculate $\alpha_2 x^2$, where x represents the time-domain counterpart of the spectrum in Fig. 3(c). That is, we convolve this spectrum with itself, group all of the terms that land at $\omega_1 - \omega_2$, and multiply the result by α_2. We thus write in the frequency domain

$$\begin{aligned} V_{M,\mathrm{IM2}}(\omega_1-\omega_2) &= \alpha_2 \frac{|V_M(\omega_1)|}{2}\frac{|V_M(\omega_2)|}{2}\delta(\omega_1-\omega_2) \\ &\quad \times \sum_{k=0}^{\infty} \frac{2}{(2k+1)^2} \\ &\cong \frac{\alpha_2\pi^2}{16}|V_M(\omega_1)|^2\,\delta(\omega_1-\omega_2) \end{aligned} \quad (15)$$

where $|V_M(\omega_1)| \approx |V_M(\omega_2)|$ denotes the amplitude of the main tones at node M and, from (12), is equal to $(V_0/\alpha_1)(|Z_4|/R_S)$. In the time domain, therefore

$$V_{\mathrm{out,IM2}}(t) = \frac{\alpha_2\pi^2}{8}\frac{V_0^2}{\alpha_1^2}\frac{|Z_4|^2}{R_S^2}\cos(\omega_1-\omega_2)t. \quad (16)$$

D. Overall IM_2 Calculation

In our final step, we add (16) to the amplified IM_2 component and equate the result to $V_{\mathrm{IM2}}\cos[(\omega_1-\omega_2)t+\theta]$, i.e.,

$$\begin{aligned} &\frac{\alpha_2\pi^2}{8}\frac{V_0^2}{\alpha_1^2}\frac{|Z_4(\omega_1)|^2}{R_S^2}\cos(\omega_1-\omega_2)t \\ &\quad - \frac{\alpha_1}{1+\alpha_1}V_{\mathrm{IM2}}\cos\left[(\omega_1-\omega_2)t+\theta+\beta\right] \\ &\quad = V_{\mathrm{IM2}}\cos\left[(\omega_1-\omega_2)t+\theta\right] \end{aligned} \quad (17)$$

when the spacing between the two tones, i.e., $\omega_1 - \omega_2$, is small. Since α_1 is large, we can assume $\alpha_1/(1+\alpha_1) \approx 1$, arriving at

$$|V_{\mathrm{IM2}}| = \frac{\alpha_2\pi^2 V_0^2\,|Z_4(\omega_1)|^2}{16\alpha_1^2 R_S^2}. \quad (18)$$

The key result here is that $|V_{\mathrm{IM2}}| \propto |Z_4(\omega_1)|^2/R_S^2$, as was the case in the continuous-time approximation. Thus, the IP_2 rises by the factor that the MBPF attenuates the blockers at ω_1 and ω_2. We can observe that $|V_{\mathrm{IM2}}|$ in (18) is attenuated by α_1^2 rather than by α_1^3 in (6). This is because $Z_F(\omega_1-\omega_2)$ approaches R_F with discrete-time feedback, but zero in continuous-time feedback.

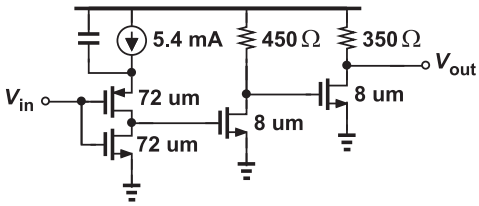

Fig. 4. Actual low-noise amplifier (LNA) topology ($L = 60$ nm).

Our derivation of (18) has made two simplifying assumptions, namely, $(1+\alpha_1)R_S = R_F$ and $|\omega - \omega_{\mathrm{LO}}|^2 \gg 1/[2(1+\alpha_1)R_S C_F]^2$, which may not hold if the open-loop gain α_1 is not very large. It is possible to repeat the analysis without these conditions; (9) leads to

$$\frac{V_{\mathrm{out}}}{V_{\mathrm{in}}} = \frac{4}{\pi^2}\frac{2(1+\alpha_1)}{1+\eta+4j(1+\alpha_1)R_S C_F(\omega-\omega_{\mathrm{LO}})} \quad (19)$$

where $\eta = (1+\alpha_1)R_S/R_F$. With the IM_2 returning to the virtual ground, (14) must be revised as

$$V_{M,\mathrm{IM2}}(t) = \frac{R_S}{R_F}V_{\mathrm{IM2}}\cos\left[(\omega_1-\omega_2)t+\theta+\beta\right]. \quad (20)$$

Writing (17) without the simplifications

$$\begin{aligned} &\frac{\alpha_2\pi^2}{8}\frac{V_0^2}{\alpha_1^2}\frac{16}{\pi^4}\frac{4(1+\alpha_1)^2\cos(\omega_1-\omega_2)t}{[1+\eta]^2+[4(1+\alpha_1)R_S C_F(\omega-\omega_{\mathrm{LO}})]^2} \\ &\quad - \frac{\alpha_1 R_S}{R_F}V_{\mathrm{IM2}}\cos\left[(\omega_1-\omega_2)t+\theta+\beta\right] \\ &\quad = V_{\mathrm{IM2}}\cos\left[(\omega_1-\omega_2)t+\theta\right]. \end{aligned} \quad (21)$$

This yields a more accurate output IM_2, i.e.,

$$|V_{\mathrm{IM2}}| \approx \frac{\alpha_2\pi^2}{8(1+\eta)}\frac{V_0^2}{\alpha_1^2}\frac{16}{\pi^4}\frac{4(1+\alpha_1)^2}{[1+\eta]^2+[4\eta R_F C_F(\omega-\omega_{\mathrm{LO}})]^2}. \quad (22)$$

We note that (18) provides insight while (22) has higher precision.

VI. Simulation Results

In order to verify the results of our IM_2 analysis, we have carried out a multitude of simulations in Cadence. This section summarizes our findings. We have chosen the values in Fig. 1(b) as follows: $R_S = 50\,\Omega$, $R_F = 1\,\mathrm{k}\Omega$, $f_{\mathrm{LO}} = 2.5$ GHz, and an N-path network consisting of four 10-pF capacitors. The uncompressed voltage gain of the amplifier is $\alpha_1 \approx 27$, yielding an RF channel bandwidth of about 12 MHz.

In the first test, we apply two tones at $f_1 = 2.520$ GHz and $f_2 = 2.522$ GHz, each having a peak amplitude of $V_0 = 6.3$ mV. This test is run on the following: 1) a behavioral amplifier (a voltage-controlled voltage source) with $\alpha_1 = 27$ and $\alpha_2 = 440\ V^{-1}$ and 2) the actual amplifier topology (65-nm CMOS technology with a 1.2-V supply) shown in Fig. 4, which

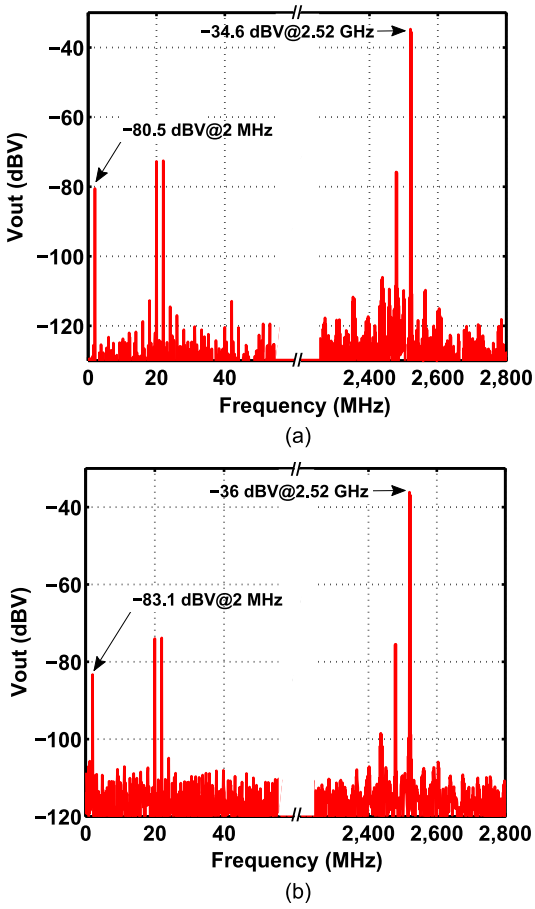

Fig. 5. Frequency spectrum of the (a) behavioral amplifier and the (b) actual amplifier.

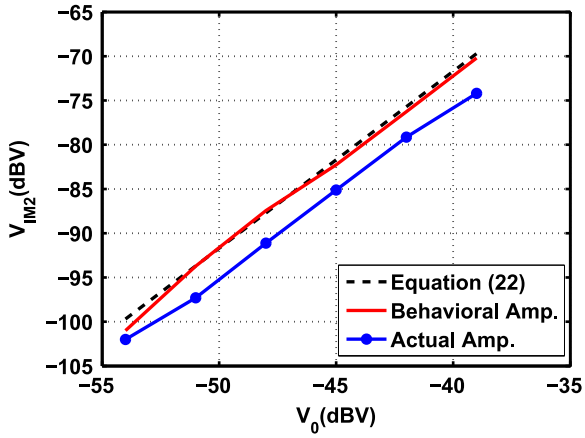

Fig. 6. V_{IM2} as a function of V_0.

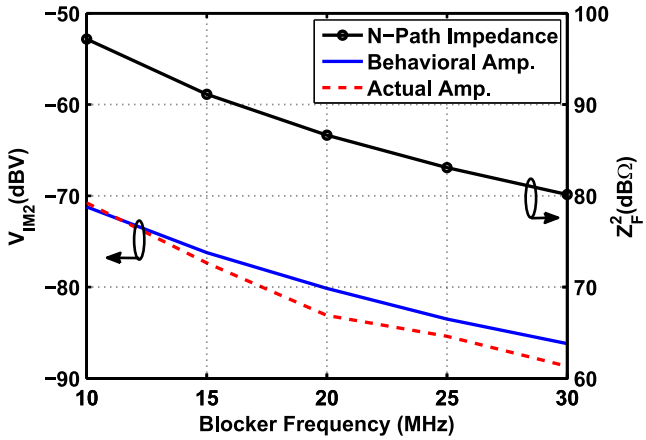

Fig. 7. V_{IM2} and $|Z_F|^2$ as a function of blocker offset frequency.

also has $\alpha_1 = 27$ and $\alpha_2 = 440\ V^{-1}$. The amplifier output spectra for the two cases are plotted in Fig. 5.

We observe that the former yields an IM_2 amplitude of -80.5 dBV, about 0.5 dB lower than (22). The latter gives a value of -83.1 dBV, which is 3.1 dB lower than (22). This discrepancy is attributed to the input capacitance of the LNA ($\approx$140 fF), which has not been included in the nonlinearity analysis.

In the second test, we increase the amplitude of the two tones from 4 to 22.4 mV_p, noting from (22) that V_{IM2} should grow proportional to V_0^2. Fig. 6 plots the simulated results against this prediction, implying good agreement.

In the third test, we sweep the tone frequencies while maintaining a 2-MHz separation, thereby exercising different parts of the front-end frequency response, i.e., different values of $|Z_F|^2$ in (18). The IM_2 behavior is depicted in Fig. 7 along with $|Z_F|^2$, revealing a constant difference in decibels from 10- to 30-MHz offset.

VII. Conclusion

The MBPF technique not only allows narrow-band filtering and blocker rejection but also improves the IP_2 of single-ended or differential front ends. In this brief, we have employed an approximation to analyze the dynamic nonlinearities of the MBPF, concluding that the IP_2 rises by the same amount that closely spaced blockers are attenuated.

References

[1] J. W. Park and B. Razavi, "Channel selection at RF using Miller band-pass filters," *IEEE J. Solid-State Circuits*, vol. 49, no. 12, pp. 3063–3078, Dec. 2014.

[2] B. D. Smith, "Analysis of commutated networks," *IRE Trans. Prof. Group Aeronaut. Navigat. Electron.*, vol. PGAE-10, pp. 21–26, Dec. 1953.

[3] W. Cheng, A. J. Annema, J. A. Croon, D. B. M. Klaasen, and B. Nauta, "A general weak nonlinearity model for LNAs," in *Proc. IEEE Custom Integr. Circuits Conf.*, Sep. 2008, pp. 221–224.

[4] J. Bussgang, L. Ehrman, and J. W. Graham, "Analysis of nonlinear systems with multiple inputs," *Proc. IEEE*, vol. 62, no. 8, pp. 1088–1119, Aug. 1974.

[5] A. Mirzaei *et al.*, "A 65 nm CMOS quad-band saw-less receiver SoC for GSM/GPRS/EDGE," *IEEE J. Solid-State Circuits*, vol. 46, no. 4, pp. 950–964, Apr. 2011.

[6] A. Homayoun and B. Razavi, "A low-power CMOS receiver for 5-GHz WLAN," *IEEE J. Solid-State Circuits*, vol. 50, no. 5, pp. 630–643, May 2015.